


Exact Potential Energy Surface for Molecules in Cavities

Lionel Lacombe,¹ Norah M. Hoffmann,^{2,1} and Neepta T. Maitra^{1,3}¹*Department of Physics and Astronomy, Hunter College of the City University of New York,
695 Park Avenue, New York, New York 10065, USA*²*Max Planck Institute for the Structure and Dynamics of Matter and Center for Free-Electron Laser Science and
Department of Physics, Luruper Chaussee 149, 22761 Hamburg, Germany*³*Physics Program and Chemistry Program, Graduate Center of the City University of New York, New York 10016, USA* (Received 31 May 2019; published 22 August 2019)

We find and analyze the exact time-dependent potential energy surface driving the proton motion for a model of cavity-induced suppression of proton-coupled electron transfer. We show how, in contrast to the polaritonic surfaces, its features directly correlate to the proton dynamics and we discuss cavity modifications of its structure responsible for the suppression. The results highlight the interplay between nonadiabatic effects from coupling to photons and coupling to electrons and suggest caution is needed when applying traditional dynamics methods based on polaritonic surfaces.

DOI: [10.1103/PhysRevLett.123.083201](https://doi.org/10.1103/PhysRevLett.123.083201)

Impressive experimental advances [1–5] have led to a rekindling of interest in cavity quantum electrodynamics. Rapidly expanding applications to molecules and nanostructures require going beyond the simplest few-level-single-mode models explored in the early days of quantum mechanics, with the interplay of coupled electronic, nuclear, and photonic excitations revealing a plethora of new phenomena, from enhanced conductivity and superconductivity to photochemical suppression of chemical reactions to superradiance; see, e.g., Refs. [6–12]. There is the possibility to manipulate matter with cavity parameters providing tunable dials for photochemical control of reactions, replacing shaped laser pulses as photonic reagents [1,13,14]. The hope is to attain strong light-matter coupling and control without large power sources, reducing unintended by-products such as multiphoton absorption and ionization channels.

The cavity clearly modifies the potential that the matter evolves in, and various constructs have been put forward to serve in lieu of the Born-Oppenheimer (BO) surfaces that have proved so instrumental for understanding cavity-free dynamics. In particular, “polaritonic surfaces” that arise from diagonalizing the electron-photon Hamiltonian parametrized by nuclear coordinates have been instructive in interpreting some of the novel phenomena mentioned above [15–19]. Another construct is the “cavity-BO surfaces” where the photonic displacement field and nuclear coordinates are treated on the same footing [7,20]. A complete dynamical picture of how the electrons and photons influence the nuclear dynamics can only be obtained when several of such surfaces in the chosen manifold together with their couplings are considered: typically, at a given time, the nuclear wave packet locally straddles several surfaces or has distinct parts associated

with different surfaces. Going beyond using the surfaces for qualitative interpretation, and implementing them in dynamics schemes, couplings between the surfaces must be included [8,21], and nonadiabatic effects arising from photon-matter coupling interplay with electron-nuclear couplings. Practical necessity calls for approximations which work best when this choice of surfaces in some sense represents a “zeroth-order” picture. The situation somewhat mirrors that for a molecule driven by classical light, where, for example, in surface-hopping schemes sometimes Floquet states (which are the classical-light analogues to the polaritonic surfaces) work best [22,23], while in other cases quasistatic (a.k.a. instantaneous BO) states are argued to be more appropriate [24,25].

The exact factorization approach (EFA) bypasses these questions while also shedding light on them. Originally presented for coupled electron-nuclear systems, a single time-dependent potential energy surface (TD PES) replaces the manifold of static surfaces and represents the exact potential that the nuclear wave packet evolves in, which exactly contains the effects of coupling to the electrons [26,27]. Generalizations of EFA have been made to include photons [28,29]. Explicit examples of how coupling to photons affects features of the potential driving an electron are given in Ref. [29], while Ref. [28] finds the exact photon-matter coupling-induced corrections to the potential driving the photons. So far, how the presence of the cavity modifies the potential driving the nuclei has not been explored. In this Letter, we find the exact cavity-modified TD PES for a model that demonstrates suppression of photo-induced proton-coupled electron transfer (PCET), a key process in energy conversion in biological and chemical systems. In contrast to polaritonic surfaces, its features alone indicate the suppression phenomenon, and it

provides the exact, unambiguous force on the nuclei to be used in mixed quantum-classical methods.

The minimal model of Refs. [30–32] has been remarkably instructive for studying nonadiabatic effects in cavity-free PCET [31–34]. The Hamiltonian involves one electron and one proton moving between two fixed ions separated by L in one dimension

$$\hat{H}_m = \hat{T}_n + \hat{H}_{\text{BO}} = \hat{T}_n + \hat{T}_e + \hat{V}_m, \quad (1)$$

where $\hat{T}_n = -(1/2M)(\partial^2/\partial R^2)$, $\hat{T}_e = -\frac{1}{2}(\partial^2/\partial r^2)$, and

$$\hat{V}_m = \sum_{\sigma=\pm 1} \left(\frac{1}{|R + \frac{\sigma L}{2}|} - \frac{\text{erf}(\frac{|r + \frac{\sigma L}{2}|}{a_\sigma})}{|r + \frac{\sigma L}{2}|} \right) - \frac{\text{erf}(\frac{|R-r|}{a_f})}{|R-r|}, \quad (2)$$

where we chose $L = 19.0$ a.u., $a_{+1} = 3.1$ a.u., $a_{-1} = 4.0$ a.u., $a_f = 5.0$ a.u., and proton mass $M = 1836$ a.u. Atomic units ($\hbar = e^2 = m_e = 1$) are used throughout. Changing these parameters changes the strength of the electron-nuclear couplings and eigenstates; a closely related model [31,32] was used to study sequential versus concerted PCET mechanisms in solvents, while a two-dimensional version was used to model a conical intersection [35].

The top panel in Fig. 1 shows the BO surfaces for the cavity-free system. Considering an initial sudden vertical electronic excitation out of the ground-state donor well on the left to the first excited BO state, the nuclear wave packet slides down the surface and splits soon after encountering the avoided crossing (see the figures shortly and movie in the Supplemental Material [36]). The part of the nuclear wave packet evolving on the lower surface then becomes associated with an electron transfer as evident from comparing the conditional BO electronic wave functions shown in the insets in Fig. 1. To investigate how placing the molecule in a cavity affects the PCET, we consider the nonrelativistic photon-matter Hamiltonian in the dipole approximation in the Coulomb gauge [19,20,28,37,38]

$$\hat{H} = \hat{H}_m + \hat{H}_p + \hat{V}_{pm} + \hat{V}_{\text{dipSE}}, \quad (3)$$

where, for a single cavity mode of frequency ω_α ,

$$\hat{H}_p(q) = \frac{1}{2}(\hat{p}_\alpha^2 + \omega_\alpha^2 \hat{q}_\alpha^2) \quad \text{and} \quad \hat{V}_{pm} = \omega_\alpha \lambda_\alpha \hat{q}_\alpha (R - r), \quad (4)$$

where $\hat{q}_\alpha = \sqrt{1/2\omega_\alpha}(\hat{a}_\alpha^\dagger + \hat{a}_\alpha)$ is the photonic displacement-field coordinate, related to the electric displacement operator, while \hat{p}_α is proportional to the magnetic field. The coupling strength $\lambda_\alpha = \lambda$ generally depends on the mode function of the cavity, but here we take it constant, assuming that the cavity is much longer than the spatial range of the molecular dynamics. The dipole self-energy

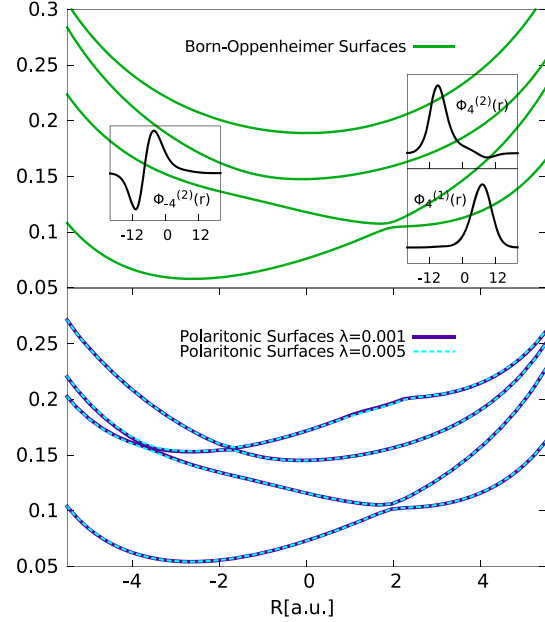


FIG. 1. Upper panel: the lowest BO surfaces for the PCET model. The initial conditional electronic wave function associated with the initial excitation on the donor side is shown in the inset on the left, showing localization of the electron at negative r values, while those associated with the BO surfaces after a proton transfer are shown on the right. The latter show that on the second surface the electron is localized at negative r values, while on the lower surface the electron becomes localized at positive r . Lower panel: the polaritonic surfaces, for coupling strengths indicated.

$\hat{V}_{\text{dipSE}} = \frac{1}{2}[\lambda_\alpha(R - r)]^2$ has a negligible effect in all cases studied. Polaritonic surfaces, defined by the eigenvalues of $\hat{H} - \hat{T}_n$, are shown in the lower panel of Fig. 1 for $\omega_\alpha = 0.1$ a.u. and $\lambda = 0.005$ a.u. and 0.001 a.u. Immediately evident is the increased number of avoided crossings compared to the BO surfaces, as nonadiabatic effects from photon-matter and electron-nuclear couplings come into play.

Turning to the dynamics, the lower part of the upper six panels in Fig. 2 shows time snapshots of the nuclear density (red) resulting from the initial wave function, $\Psi(r, q, R, 0) = \mathcal{N}e^{-[(R+4)^2/2.85]}\Phi_R^{\text{BO}(2)}(r)\xi^{(0)}(q)$, where $\xi^{(0)}(q) = (\omega_\alpha/\pi)^{1/4}e^{-\omega_\alpha q^2/2}$ is the zero-photon state in the cavity. The figure and movie in the Supplemental Material [36] demonstrate cavity-induced suppression of PCET: significantly less proton density moves to the right compared to the cavity-free case (black), and while the electron transfers in concert with the proton transfer in cavity-free dynamics (see black dipoles in the lowest right panel), it is partially suppressed when the molecule is placed in the cavity with $\lambda = 0.005$ a.u. The snapshots show that part of the wave packet becomes trapped on the left, reducing the nuclear dipole moment and consequently reducing the electron transfer.

Attempting to understand the suppression from the shape of the polaritonic surfaces (Fig. 1) alone is impossible: one

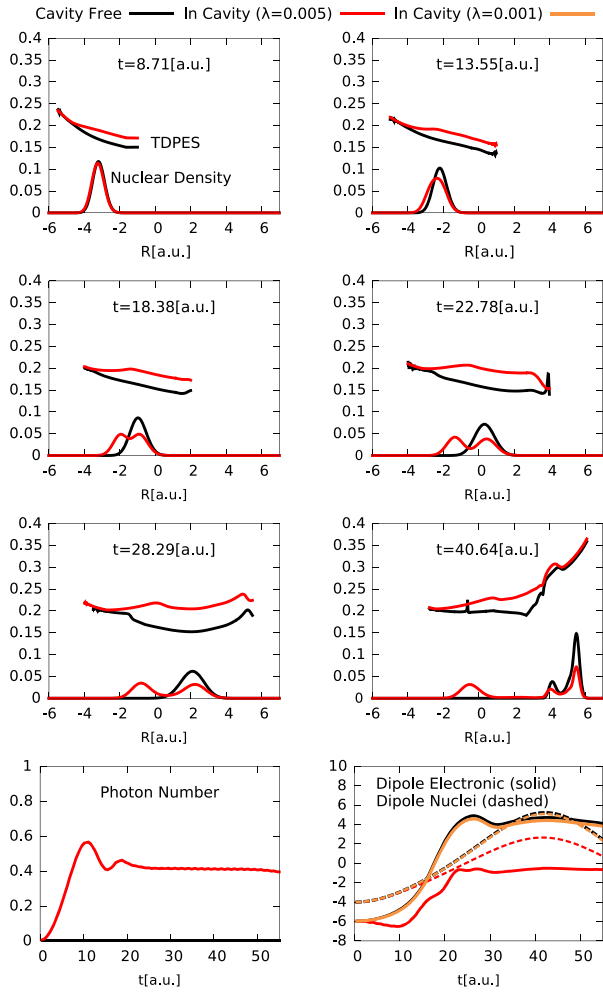


FIG. 2. Snapshots of the nuclear density (scaled by 0.1) and exact TD PES for dynamics inside (red) and outside (black) the cavity. The lowest panels show the electronic and nuclear dipole moments and the photon number over time. Cavity-induced suppression of PCET is evident in the red density as part of the nuclear wave packet becomes trapped on the left, consistent with the structure of the TD PES (see text).

might be tempted to attribute the partial trapping of the density to the barrier in the third polaritonic surface at around $R \approx -2$ a.u.; however not only does the trapped density evolve past this point, but also the barrier is present in the weaker coupling $\lambda = 0.001$ a.u. case which shows negligible suppression as indicated by the orange dipole shown in the lowest panel of Fig. 2 and movie in the Supplemental Material [36]. Instead, as we shortly discuss, the structure of the exact TD PES shown in Fig. 2 directly correlates with the dynamics.

The TD PES is a fundamental construct arising from the EFA [26,27]. When extended to systems of coupled electrons, nuclei, and photons [28,29], EFA factorizes the complete wave function into a nuclear wave function $\chi(R, t)$ and a conditional electron-photon wave function $\Phi_R(r, q, t)$, $\Psi(r, q, R, t) = \chi(R, t)\Phi_R(r, q, t)$, in which the exact equation for the marginal $\chi(R, t)$ is Schrödinger,

$$\{-[\nabla + A(R, t)]^2/2M + \epsilon(R, t)\}\chi(R, t) = i\partial_t\chi(R, t), \quad (5)$$

(written here for one nuclear coordinate), with a scalar potential, the TD PES $\epsilon(R, t)$, and a vector potential $A(R, t)$, both of which depend on $\Phi_R(r, q, t)$. The time evolution for the latter is more complicated [39], with a $\chi(R, t)$ -dependent non-Hermitian operator that operates on the R dependence of $\Phi_R(r, q, t)$. The exact equations are provided in the Supplemental Material [36]. The roles of the nuclei, electrons, and photons can be permuted in EFA such that the subsystem of most interest is chosen for the marginal factor χ since this satisfies the Schrödinger equation [28], e.g., choosing the photonic system as the marginal, Ref. [28] found distortions of the exact potential driving the photonic field away from harmonic due to photon-matter coupling.

The factorization of Ψ is unique up to an (R, t) -dependent phase-factor multiplying $\chi(R, t)$ with its inverse multiplying $\Phi_R(r, q, t)$; this in turn transforms the potentials, and for one nuclear dimension, a gauge can always be found in which $A(R, t)$ is zero. Then, the only potential driving the nuclei is $\epsilon(R, t)$ and, for the cavity-enclosed PCET model, is shown in the time snapshots of Fig. 2. Comparing with the cavity-free TD PES, the structures that lead to the partial trapping of the nuclear density, and the subsequent partial PCET suppression, are clearly seen. At early times, the slope of the TD PES is smaller compared to the cavity-free case, even sloping upward in the trailing part of wave packet, therefore slowing down and spreading out the wave packet compared to the cavity-free case (up to $t = 13.55$ a.u.). A gentle step develops, lowering the potential on the left of the wave packet, which begins to split the wave packet in two parts ($t = 18.38$ a.u.): one associated with TD PES turning downward and forming a well to the left and the other turning downward to the right, further enhancing the splitting. The nuclear wave packet on the left becomes trapped in the well, and eventually oscillates in it, unable to reach the region of electron-nuclear nonadiabatic coupling that leads to the electron transfer. In contrast, the nuclear wave packet on the right continues moving to the right ($t = 22.78, 28.29$ a.u.), where it later splits and behaves similarly to the cavity-free dynamics but scaled down since some density was lost in the trapped region on the left ($t = 40.64$ a.u.).

The shape of the TD PES therefore directly reflects the proton's dynamics. To understand the physical mechanisms yielding its shape, we consider the TD PES against the backdrop of polaritonic surfaces. First, we decompose the surface into weighted polaritonic (wpol), kinetic (kin), and gauge-dependent (GD) components that arise from the form of the EFA [27,28] (see the Supplemental Material [36]),

$$\epsilon(R, t) = \epsilon_{\text{wpol}}(R, t) + \epsilon_{\text{kin}}(R, t) + \epsilon_{\text{GD}}(R, t), \quad (6)$$

$$\epsilon_{\text{wpol}}(R, t) = \langle \Phi_R | \hat{H}_{\text{BO}} + \hat{H}_p + \hat{V}_{pm} | \Phi_R \rangle_{r,q}, \quad (7)$$

$$\epsilon_{\text{kin}}(R, t) = \langle \Phi_R | -\nabla_R^2 \Phi_R \rangle_{r,q} / 2M, \quad (8)$$

$$\epsilon_{\text{GD}}(R, t) = \langle \Phi_R | -i\partial_t \Phi_R \rangle_{r,q}. \quad (9)$$

In Fig. 3, we plot $\epsilon_{\text{wpol}}(R, t)$ and $\epsilon_{\text{GD}}(R, t)$ against the backdrop of the static polaritonic surfaces; ϵ_{kin} remains negligible throughout, due to the $1/M$ prefactor. At early times we observe that ϵ_{wpol} on the left lies intermediate between the second and third polaritonic surfaces, acquiring a mixed character, while on the right adheres to the second surface. Looking at the middle row, this behavior resolves into the left part of the nuclear wave packet being correlated with the third polaritonic surface, while the right correlates with the second: this piecewise behavior illustrates matter-photon correlation, with the left part correlated with photon emission accompanying an electronic transition to the lower BO surface (see also Fig. 4 shortly), while the right part of the nuclear wave packet is correlated with a zero-photon electronically excited state. The step in ϵ_{wpol} that bridges the

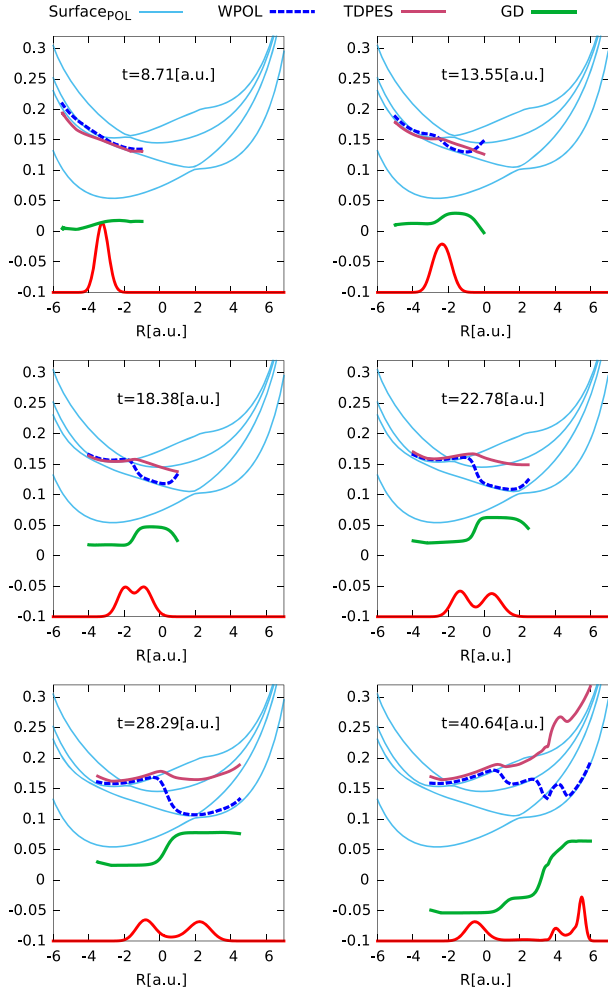


FIG. 3. Snapshots of the nuclear density and the components of the TD PES for dynamics in the cavity, $\lambda = 0.005$, $\omega_\alpha = 0.1$. The thin lines represent the polaritonic surfaces.

two polaritonic surfaces after the photon-emission event is analogous to that found in earlier work between BO surfaces [33] and between Floquet surfaces [23], which polaritonic surfaces reduce to in the classical-light limit [40]. Also analogous is that ϵ_{GD} displays a countering step [34], that adjusts the energy locally in the nuclear system to account for the different energies of the electron-photon system associated with the different characters on the left and right. It is important to note that the suppression mechanism sets in during the stage when the surface has mixed character, before the piecewise-shifted character of ϵ_{GD} sets in. This is also well before part of the wave packet encounters the avoided crossing associated with strong electron-nuclear coupling around $R \approx 2$ a.u. (see also the BO surfaces Fig. 1), which is where the nuclear wave packet splits again with the part moving to the lowest surface associated with the electron moving to the lowest surface associated with the electron transfer. At the final time shown we see three parts to the nuclear wave packet: the left part trapped in the left well associated with a one-photon BO ground state, and two lobes on the right, with the extreme right associated with PCET on the BO ground state, and the other with the excited BO state, both with zero photons. The ϵ_{wpol} component of the TD PES directly reflects this matter-polariton correlation, while ϵ_{GD} adjusts the local energy in a piecewise manner.

To further clarify the dynamics in the conditional variables q and r , Fig. 4 shows the n photon resolved nuclear density, defined as

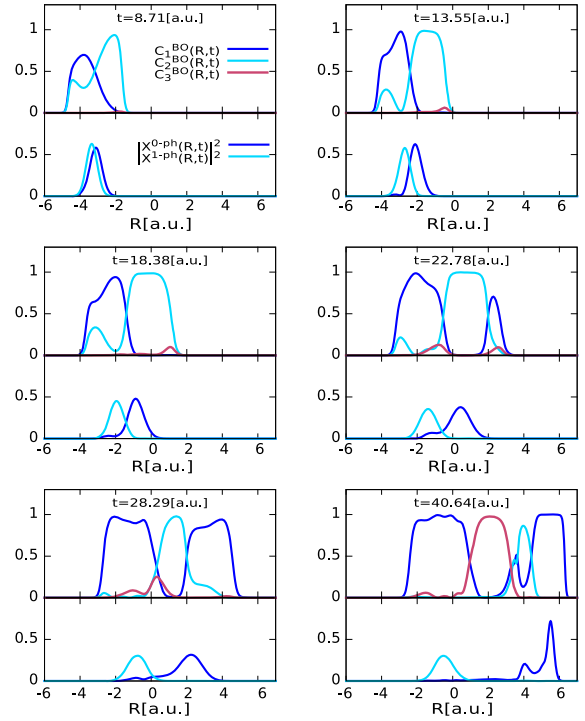


FIG. 4. Snapshots of the zero- and one-photon resolved nuclear densities of Eq. (10) (lower panel), along with the BO coefficients of Eq. (11) (upper panel).

$$|\chi^{n-ph}(R, t)|^2 = |\langle \xi_n | \Psi(t) \rangle_{r,q}|^2, \quad (10)$$

where $\xi_n(q)$ are the harmonic oscillator eigenstates of H_p , and the BO coefficients, defined as

$$C_i^{\text{BO}}(R, t) = |\langle \Phi_R^{\text{BO},i} | \Psi(t) \rangle_{r,q}|^2 / |\chi(R, t)|^2. \quad (11)$$

These measures clearly show the nuclear-photon and nuclear-electron correlations throughout the evolution (see also movie in the Supplemental Material [36]). At early times there is mixed character of the electron-photon state, with both zero-photon and one-photon contributions associated with the nuclear density at a given R , and fractional BO coefficients contributing with occupation even in the third BO state. At later times local regions of the nuclear density become correlated with different electronic and photonic characters.

In conclusion, we analyzed the structure of the TDPEs for a model of PCET and have shown how its features predict the cavity-induced suppression. While polaritonic surfaces provide a useful backdrop, they are not able to predict dynamics or mechanisms without considering their couplings to each other in dynamics [8,9], and care is needed with such dynamics schemes, due to the propensity of near crossings caused by both electron-nuclear and matter-photon couplings. For mixed quantum-classical methods, which would be required for many-molecule systems [21,41], overcoherence in surface-hopping methods is likely to be quite problematic. Instead, this work shows the promise of rigorously based mixed quantum-classical approximations for cavity-qed, based on, for example, generalizations of the schemes of Refs. [42–49], that have been successful for cavity-free nonadiabatic dynamics.

Financial support from the U.S. National Science Foundation CHE-1566197 (L.L.) and the Department of Energy, Office of Basic Energy Sciences, Division of Chemical Sciences, Geosciences and Biosciences under Award No. DE-SC0015344 (N.T.M) is gratefully acknowledged. N.M.H. gratefully acknowledges funding from the Max-Planck Institute for the Structure and Dynamics of Matter, and an IMPRS fellowship.

-
- [1] T. W. Ebbesen, *Acc. Chem. Res.* **49**, 2403 (2016).
 [2] B. Barnes, F. García Vidal, and J. Aizpurua, *ACS Photonics* **5**, 1 (2018).
 [3] P. Vasa and C. Lienau, *ACS Photonics* **5**, 2 (2018).
 [4] D. G. Baranov, M. Wersäll, J. Cuadra, T. J. Antosiewicz, and T. Shegai, *ACS Photonics* **5**, 24 (2018).
 [5] J. T. Hugall, A. Singh, and N. F. van Hulst, *ACS Photonics* **5**, 43 (2018).
 [6] E. Orgiu, J. George, J. A. Hutchison, E. Devaux, J. F. Dayen, B. Doudin, F. Stellacci, C. Genet, J. Schachenmayer,

- C. Genes, G. Pupillo, P. Samori, and T. W. Ebbesen, *Nat. Mater.* **14**, 1123 (2015).
 [7] J. Flick, M. Ruggenthaler, H. Appel, and A. Rubio, *Proc. Natl. Acad. Sci. U.S.A.* **114**, 3026 (2017).
 [8] M. Kowalewski, K. Bennett, and S. Mukamel, *J. Phys. Chem. Lett.* **7**, 2050 (2016).
 [9] M. Kowalewski and S. Mukamel, *Proc. Natl. Acad. Sci. U.S.A.* **114**, 3278 (2017).
 [10] F. Herrera and F. C. Spano, *Phys. Rev. Lett.* **116**, 238301 (2016).
 [11] G. Mazza and A. Georges, *Phys. Rev. Lett.* **122**, 017401 (2019).
 [12] M. A. Sentef, M. Ruggenthaler, and A. Rubio, *Sci. Adv.* **4**, eaau6969 (2018).
 [13] R. F. Ribeiro, L. A. Martinez-Martinez, M. Du, J. Campos-Gonzalez-Angulo, and J. Yuen-Zhou, *Chem. Sci.* **9**, 6325 (2018).
 [14] A. Csehi, A. Halasz, G. J. Vibok, and M. Kowalewski, *arXiv:1904.12693*.
 [15] J. Galego, F. J. Garcia-Vidal, and J. Feist, *Phys. Rev. X* **5**, 041022 (2015).
 [16] J. Galego, F. J. Garcia-Vidal, and J. Feist, *Nat. Commun.* **7**, 13841 (2016).
 [17] J. Feist, J. Galego, and F. J. Garcia-Vidal, *ACS Photonics* **5**, 205 (2018).
 [18] C. Schäfer, M. Ruggenthaler, H. Appel, and A. Rubio, *Proc. Natl. Acad. Sci. U.S.A.* **116**, 4883 (2019).
 [19] M. Ruggenthaler, N. Tancogne-Dejean, J. Flick, H. Appel, and A. Rubio, *Nat. Rev. Chem.* **2**, 0118 (2018).
 [20] J. Flick, H. Appel, M. Ruggenthaler, and A. Rubio, *J. Chem. Theory Comput.* **13**, 1616 (2017).
 [21] H. L. Luk, J. Feist, J. J. Toppari, and G. Groenhof, *J. Chem. Theory Comput.* **13**, 4324 (2017).
 [22] M. Fischer, U. Lorenz, B. Schmidt, and R. Schmidt, *Phys. Rev. A* **84**, 033422 (2011).
 [23] T. Fiedlschuster, J. Handt, E. K. U. Gross, and R. Schmidt, *Phys. Rev. A* **95**, 063424 (2017).
 [24] M. Thachuk, M. Y. Ivanov, and D. M. Wardlaw, *J. Chem. Phys.* **105**, 4094 (1996).
 [25] Y. Sato, H. Kono, S. Koseki, and Y. Fujimura, *J. Am. Chem. Soc.* **125**, 8019 (2003).
 [26] A. Abedi, N. T. Maitra, and E. K. U. Gross, *Phys. Rev. Lett.* **105**, 123002 (2010).
 [27] A. Abedi, N. T. Maitra, and E. K. U. Gross, *J. Chem. Phys.* **137**, 22A530 (2012).
 [28] N. M. Hoffmann, H. Appel, A. Rubio, and N. T. Maitra, *Eur. Phys. J. B* **91**, 180 (2018).
 [29] A. Abedi, E. Khosravi, and I. V. Tokatly, *Eur. Phys. J. B* **91**, 194 (2018).
 [30] S. Shin and H. Metiu, *J. Chem. Phys.* **102**, 9285 (1995).
 [31] J.-Y. Fang and S. Hammes-Schiffer, *J. Chem. Phys.* **106**, 8442 (1997).
 [32] J.-Y. Fang and S. Hammes-Schiffer, *J. Chem. Phys.* **107**, 5727 (1997).
 [33] A. Abedi, F. Agostini, Y. Suzuki, and E. K. U. Gross, *Phys. Rev. Lett.* **110**, 263001 (2013).
 [34] F. Agostini, A. Abedi, Y. Suzuki, S. K. Min, N. T. Maitra, and E. K. U. Gross, *J. Chem. Phys.* **142**, 084303 (2015).
 [35] S. K. Min, A. Abedi, K. S. Kim, and E. K. U. Gross, *Phys. Rev. Lett.* **113**, 263004 (2014).

- [36] See Supplemental Material at <http://link.aps.org/supplemental/10.1103/PhysRevLett.123.083201> for a brief presentation of the exact factorization equations we use here, the values of numerical parameters used in the calculations, and three movies as described in the text to support the figures shown.
- [37] I. V. Tokatly, *Phys. Rev. Lett.* **110**, 233001 (2013).
- [38] M. Ruggenthaler, J. Flick, C. Pellegrini, H. Appel, I. V. Tokatly, and A. Rubio, *Phys. Rev. A* **90**, 012508 (2014).
- [39] G. H. Gossel, L. Lacombe, and N. T. Maitra, *J. Chem. Phys.* **150**, 154112 (2019).
- [40] S. Guérin, F. Monti, J.-M. Dupont, and H. R. Jauslin, *J. Phys. A* **30**, 7193 (1997).
- [41] B. Migolet and B. F. E. Curchod, *J. Phys. Chem. A* **123**, 3582 (2019).
- [42] F. Agostini, S. K. Min, A. Abedi, and E. K. U. Gross, *J. Chem. Theory Comput.* **12**, 2127 (2016).
- [43] S. K. Min, F. Agostini, and E. K. U. Gross, *Phys. Rev. Lett.* **115**, 073001 (2015).
- [44] S. K. Min, F. Agostini, I. Tavernelli, and E. K. U. Gross, *J. Phys. Chem. Lett.* **8**, 3048 (2017).
- [45] F. Agostini and B. F. E. Curchod, *Comput. Mol. Sci.* **9**, e1417 (2019).
- [46] G. H. Gossel, F. Agostini, and N. T. Maitra, *J. Chem. Theory Comput.* **14**, 4513 (2018).
- [47] J.-K. Ha, I. S. Lee, and S. K. Min, *J. Phys. Chem. Lett.* **9**, 1097 (2018).
- [48] M. Filatov, M. Paolino, S. K. Min, and C. H. Choi, *Chem. Commun.* **55**, 5247 (2019).
- [49] M. Filatov, S. K. Min, and C. H. Choi, *Phys. Chem. Chem. Phys.* **21**, 2489 (2019).